LOCALIZED MODULATION OF TURBULENCE BY MAGNETIC ISLANDS ON HL-2A TOKAMAK

M. Jiang, W. Chen, Z.B. Shi, J.Q. Li, W.L. Zhong, X.T. Ding, X.Q. Ji, P.W. Shi, Z.C. Yang, B.S. Yuan, Y.G. Li, Y. Zhou, D.L. Yu, Y. Liu, Q.W. Yang, M. Xu and HL-2A
Southwestern Institute of Physics
P.O. Box 432, Chengdu 610041, People's Republic of China
Email: jiangm@swip.ac.cn

Y. Xu
Institute of Fusion Science, School of Physical Science and Technology, Southwest Jiaotong University
Chengdu, 610031, People's Republic of China

W. Wang
Princeton University, Plasma Physics Laboratory, Theory Division MS 27,
Princeton, NJ 08543, USA

Abstract

Modulation on turbulent electron temperature fluctuations and density fluctuations by an *m/n* =1/1 tearing mode island was observed in the core plasma region of the HL-2A tokamak. High tempo-spatial resolution two-dimensional images of temperature fluctuations show that the turbulence modulation occurs only when the island width exceeds a certain threshold value (6.4 cm) and the modulation is localized merely in the inner half area of the island due to significant alteration of local profiles and turbulence drives. Evidence also reveals that for large islands turbulence spreading takes place across the flat temperature of the O-point at the inner half island region, whereas in the outer half area the small temperature gradient drives a low level of temperature fluctuations.

1. INTRODUCTION

It is well-known that magnetic islands formed in magnetically confined plasmas have significant influence on plasma profiles and cross-field transport [1-5]. They are also considered to be key ingredients at the onset of plasma disruptions [6]. On the other hand, observations of internal transport barriers near the rational magnetic surface suggest the importance of magnetic islands in plasma confinement via increase of flow shear at the island boundary [7-9]. In recent years the multi-scale interaction between large-scale modes and micro-scale turbulence has been found to play an important role in regulating turbulent transport [10-14] and eventually for the low to high mode transition [15-16]. It was reported in DIII-D that electrostatic fluctuations were modulated by m/n=2/1 neoclassical tearing mode, where the ion temperature gradient driven turbulence is reduced across the entire region of the naturally occurring, rotating island [5, 10], consistent with theoretical predictions [17]. In ref. [18], a diffusive transport model indicates an island-width threshold, only above which the magnetic island may impose effects on plasma profiles and transport, in accord with nonlinear simulations [19]. Apparently, detailed studies of interaction between macro-scale tearing modes and micro-scale turbulence are essential for further understanding the tearing instability and the island-induced transport, which will ultimately lead to developing a better control of tearing mode and optimization of plasma performance in fusion devices, such as ITER.

In this paper, we report the experimental observation of modulation of both temperature ($\tilde{T}_e$) and density fluctuations ($\tilde{n}_e$) by an *m/n* =1/1 tearing mode (TM) island in the core of the HL-2A tokamak. High temporal and spatial resolution 2D images of $\tilde{T}_e$ show clear evidence that the turbulence modulation occurs solely when the island width exceeds a certain threshold value. And the modulation is localized just in the inner half island region due to significant alteration of local profiles and turbulence drives between the X-point and O-point. The results also reveal that for large islands turbulence spreading takes place across the flattened temperature of the O-point at the inner half island, whereas in the outer half area the small temperature gradient corresponds to a low level of temperature fluctuations.

2. EXPERIMENTAL SETUP

The experiments were performed in the NBI heated plasmas in the HL-2A tokamak with a divertor configuration. The major radius $\boldsymbol{R_0}$ = 1.65 m, minor radius $a \approx$ 0.34 m, toroidal magnetic field $\boldsymbol{B_t}$ = 1.3 T,

plasma current $\boldsymbol{I_p}$ ≈ 150 kA, neutral beam power ≈ 1 MW, the central line-averaged density $\boldsymbol{\bar{n}_{e0}}$ ≈ 2 × $\boldsymbol{10^{19}}$ m^{-3} and the core electron and ion temperature is about 1.7 keV and 1.0 keV, respectively. The results reported here were mainly obtained by following diagnostics: a 24 (vertical) × 8 (radial) electron cyclotron emission imaging (ECEI) array to measure the local $\boldsymbol{T_e}$ and $\boldsymbol{\tilde{T}_e}$ in optically thick plasmas with a sampling rate of 500 kHz and spatial resolution of 1.8-2.3 cm. The view field of the image was focused at the low field side, covering a rectangular area of 40-55 cm (vertical) × 12-17 cm (radial) to capture the entire tempo-spatial evolution of the *m/n*=1/1 island structure [20]; a multi-channel ECE radiometer to detect the $\boldsymbol{T_e}$ profile and its gradient [21]. Both of the ECE and midplane ECEI channels have been cross-calibrated with core Thomson scattering diagnostic; a four-channel microwave interferometry to measure line-integral density fluctuations [22].

3. EXPERIMENTAL RESULTS AND DISCUSSIONS

In the HL-2A tokamak there are many sawtooth oscillations in a single discharge, during which the m/n = 1/1 tearing mode was observed to rotate periodically in a frequency range ≈ 3-6 kHz. Figure 1(a) shows typical time evolution of relative T_e variations ($\delta T_e/\bar{T}_e$, where $\delta T_e = T_e - \bar{T}_e$ and $\bar{T}_e$ is a time average and approximately constant for the duration of many periods) for one channel ECEI signal measured at R = 177.11 cm and Z = 3.46 cm. A representative sequence of 2D ECE images (taken at t_1, t_2, t_3, t_4 in Fig. 1(a)) is shown in Fig. 1(b) to illustrate the location and structure of the magnetic island. The white dashed curve denotes the q = 1 rational surface. As the m/n = 1/1 island structure rotates in the laboratory frame, different phases of the island were captured at different times. The first (third) image at t_1 (t_3) corresponds to the X-point (O-point) phase when the X-point (O-point) of the tearing mode island moves to the center of the ECE image [23]. The four images from time t_1 to t_4 clearly exhibit the entire structure of the m = 1 island, rotating poloidally in the ion diamagnetic drift (clockwise) direction at a frequency ~ 4.3 kHz. The island width is about 11 cm, which is estimated from the relatively flatted profile of T_e at the O-point, as shown in Fig. 5(c).

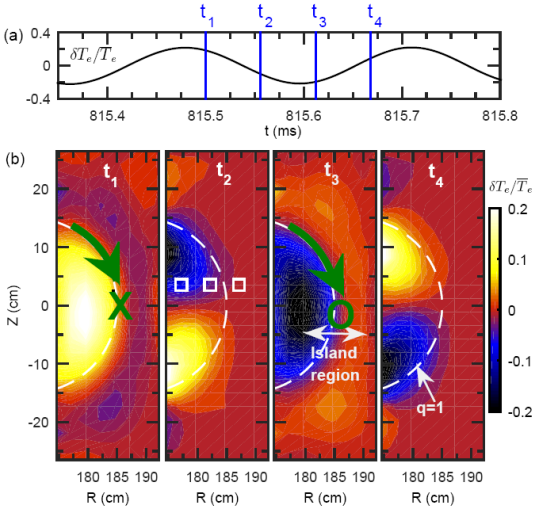

FIG. 1 (a) Time evolution of $\delta T_e/\bar{T}_e$ for one ECEI signal measured at R=177.11 cm and Z=3.46 cm (marked by the left white square in the second image of Fig. 1(b)). The signal is bandpass filtered in 3-6 kHz; (b) four ECE images taken at t_1, t_2, t_3, t_4 in Fig. 1(a), showing the clockwise rotation of the m/n=1/1 magnetic island in the time period of (815.50–815.67) ms. The X-point and O-point of the island at t_1 and t_3 are indicated with the green X and O marks, respectively. The white dashed curve denotes the location of the q =1 surface.

Plotted in Figs. 2(a)-(c) are the temporal evolution of the ECEI signal measured inside, near, and outside the q=1 surface, respectively (see three white squares in the image of Fig. 1(b) at time t_2). The vertical dashed lines denote the O-point passing-by times. When the X-point moves to the detection positions, the local T_e increases inside and nearby the q=1 surface, whereas outside that surface the local T_e decreases. In Figs. 2(a) and (c), the anti-phase behavior is seen between the T_e signals inside and outside the q=1 surface. Near the q=1 surface, the local T_e is roughly flatted across the O-point region, as shown in Fig. 2(b). As illustrated in ref. [23], this flat T_e manifests the tearing mode feature, different from an ideal kink mode.

Figures 2(d) and (e) further display the time history of electron temperature fluctuations $\tilde{T}_e$ (integrated from 20-100 kHz) measured at R = 182.14 cm and Z = 3.46 cm and chord-averaged electron density fluctuations

$\tilde{n}_e$ passing through the island region (integrated from 50-300 kHz), respectively. The envelopes of the temperature and density fluctuations are calculated via the Hilbert transform and depicted by the red curves. The fluctuation amplitudes in $\tilde{T}_e$ and $\tilde{n}_e$ are both modulated during the rotation of the *m/n* =1/1 island, i. e., minimum at the O-point and maximum at the X-point. The modulation on the envelopes is approximately in phase with the interchange of the O- and X-point, consistent with gradient-driven turbulence since in the O-point region the local T_e or n_e gradient is the minimum. Such a modulation can also be seen in the frequency spectrum of the temperature and density signals. In Figs. 3(a) and (b), the power spectra of the raw signals measured by the ECEI and the interferometry are illustrated. As expected, the coherent peak at $f \approx 4.3$ kHz in the spectra reflects the modulation on local temperature and density profiles by rotation of the *m/n* =1/1 TM island. To gain further insight into the modulation on broadband turbulence, we analyzed the envelope of temperature fluctuations ($\phi_{\tilde{T}_e}(t)$) and density fluctuations ($\phi_{\tilde{n}_e}(t)$) in the frequency range of 20-100 kHz and 50-300 kHz (see shaded areas), respectively, i.e., $\phi_{\tilde{T}_e}(t) = \left(\frac{1}{2\pi}\int_{20\ \mathrm{kHz}}^{100\ \mathrm{kHz}} \tilde{T}_e(f) e^{i2\pi f t} df\right)^2$, where $\tilde{T}_e(f)$ is the Fourier transform of $\tilde{T}_e(t)$ and $\phi_{\tilde{n}_e}(t)$ is calculated in a similar way. The frequency spectrum of the envelope $\phi_{\tilde{T}_e}(t)$ and $\phi_{\tilde{n}_e}(t)$ is shown in the inset of Figs. 3(a) and (b), respectively. Both of the envelope spectrum exhibit clear peaks at the rotating TM frequency, signifying the modulation of broadband turbulence across the island. Note that the island rotation may also induce a modulation of E_r between the X- and O-point and the $E_r \times B$ Doppler shift will shift some turbulence spectral power in and out of the frequency integration range, and hence, modulate turbulence. In our case, we have investigated such influence and found that the Doppler shift-induced turbulence modulation is very small. Similar modulation of density and temperature fluctuations by the 2/1 NTM island has been observed in DIII-D [5, 10].

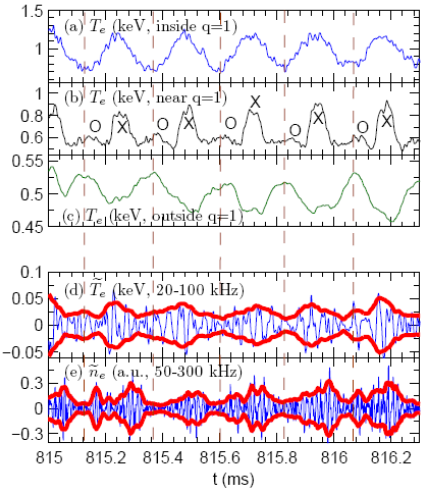

FIG. 2. Temporal evolution of the ECEI signals measured (a) inside, (b) near, and (c) outside the q=1 surface, as marked by three white squares in the image of Fig. 1(b) at time t_2. The vertical dashed lines denote the O-point passing-by times. (d) and (e) show time histories of electron temperature fluctuations $\tilde{T}_e$ (integrated from 20-100 kHz) measured at R=182.11 cm and Z=3.46 cm and chord-averaged electron density fluctuations $\tilde{n}_e$ (integrated from 50-300 kHz), respectively. The envelopes of fluctuations are depicted by the red curves.

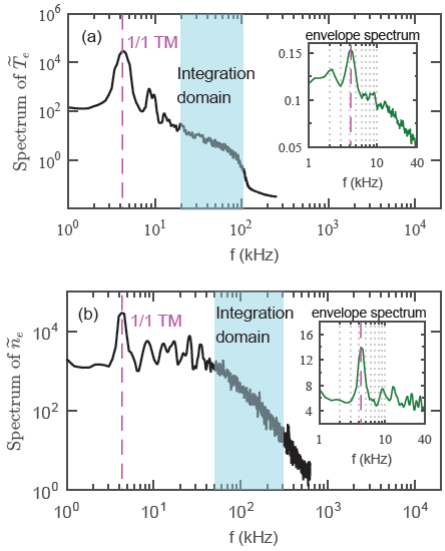

FIG. 3. Power spectrum of (a) $\tilde{T}_e$ and (b) $\tilde{n}_e$. The inset in (a) and (b) shows the amplitude spectrum of the corresponding envelope signal, $\phi_{\tilde{T}_e}(t)$ in the frequency range Δf =20-100 kHz (shaded in (a)) and $\phi_{\tilde{n}_e}(t)$ in Δf =50-300 kHz (shaded in (b)), respectively.

To investigate the three-wave coupling between tearing mode and the broadband turbulence, the squared bicoherence spectrum has been calculated, which is denoted as $b^2_{XYZ}(f_1, f_2) = \frac{\langle |X(f_1)Y(f_2)Z^*(f_1+f_2)|^2 \rangle}{\langle |X(f_1)Y(f_2)|^2 \rangle \langle |Z(f_1+f_2)|^2 \rangle}$, where $X(f), Y(f), Z(f)$ are the Fourier transform of *x(t)*, *y(t)* and *z(t)*, and $Z^*(f)$ is the complex conjugate. The squared bicoherence $b^2_{XYZ}(f_1, f_2)$ is an indicator of the strength of nonlinear coupling of three waves at f_1, f_2, and $f_1 + f_2$. Figure 4(a) shows the auto-squared bicoherence of the envelope of density fluctuations, i.e. $x(t) = y(t) = z(t) = \phi_{\tilde{n}_e}(t)$. Three noticeable peaks are observed, i.e. $f_2 \approx \pm 4.3$ kHz and $f_1 + f_2 \approx$ 4.3 kH. Similar peaked frequency is also seen in the summed bicoherence (see Fig. 4(b)), where $\sum b^2(f) = \sum_{f=f_1+f_2} b^2(f_1, f_2)/N(f)$ and *N(f)* is the number of Fourier components for each *f* in the summation. And these peaked frequencies are corresponding to the island rotating frequency observed in Fig.3, indicating there exists strong nonlinear coupling between magnetic island and turbulence.

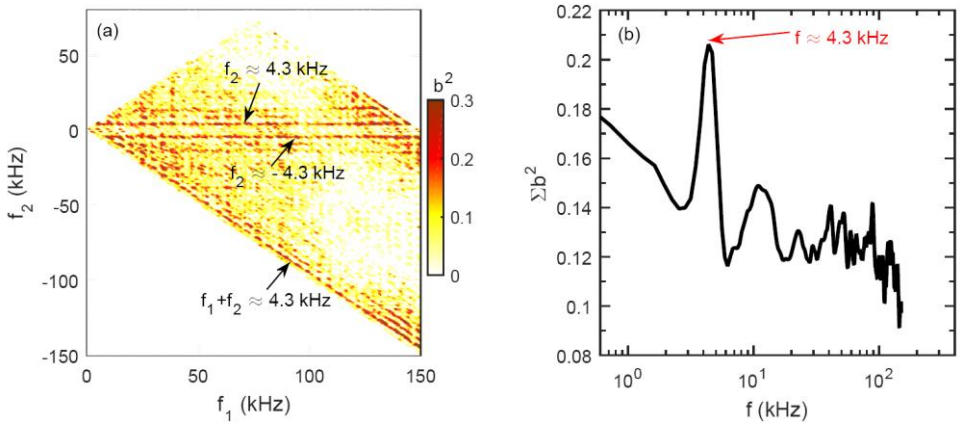

FIG. 4. (a) Contour-plot of squared auto-bicoherence of the envelope of density fluctuations $b^2(f_1, f_2)$, and (b) the summed bicoherence for each frequency f.

In this study, it is interesting to find that the 1/1 TM island modulation on micro-turbulence of $\tilde{T}_e$ emerges under certain conditions: (i) the island must be wide enough and the threshold width is about w_c= 6.4 cm in our case; (ii) for large islands, the modulation occurs only at the inner half area of the island, as marked in Fig. 5(a) by green spots of the ECEI array. Figure 5(b) shows the envelope spectra of $\tilde{T}_e$ measured by eight ECEI channels at *Z*=3.46 cm. One can clearly see that the modulation frequency peak (at $f \approx$4.3 kHz) just appears in ch5 and ch6, while for other six channels there is no TM frequency peak emerged in their envelope spectra. These results reveal that the turbulence modulation by rotating islands may take place only at certain region of the island, but not across the entire island, which is different from that observed in DIII-D [10]. To investigate

the underlying physics, we compare the radial profiles of T_e between the X-point and the O-point, as plotted in Fig. 5(c). The profiles were measured by a multi-channel ECE radiometer in a wider radial range than the ECEI and the data are phase-lock averaged over 100 cycles of X- and O-points. In case of the X-point, the T_e increases monotonically from the plasma edge to the center. For the O-point the T_e is, in general, flatted inside the island. However, at the inner half region (179 cm < R < 185 cm) the T_e is much flatter than at the outer half area (185 cm < R < 190 cm). Similar "uneven" T_e profile has also been observed in DIII-D [5]. As such, the difference of the local T_e gradient between the X-point ($\nabla T_e(X)$) and O-point ($\nabla T_e(O)$) is much more pronounced in the inner half island than the outer half. The ratio of $\nabla T_e(X)/\nabla T_e(O)$ is plotted in Fig. 5(d) as a function of the island width (w). For small TM islands, the variation of ∇T_e from the X-point to the O-point is minor, and thus, the value of $\nabla T_e(X)/\nabla T_e(O)$ is quite small when w < 6.4 cm. The critical island width (W_c) required for the T_e "flattening" has been estimated in the analytical study [18], which gives $W_c = 4\Delta_c \approx 4\left(\frac{\chi_\perp}{\chi_\parallel}\right)^{\frac{1}{4}}\left(\frac{L_s}{k_\theta}\right)^{\frac{1}{2}} \approx 4\left(\frac{\rho_s^2 C_s}{a k_\parallel' V_{the}}\right)^{\frac{1}{3}} \approx 5.1$ cm using the parameters at HL-2A. Here, ρ_s, C_s, a, $k_\parallel'$ and V_{the} are the Larmor radius at sound speed, sound speed, minor radius, radial gradient of parallel wavenumber and electron thermal velocity, respectively. The experimental observation is therefore rather close to that predicted by the theoretical model. With the increase of the island width, the value $\nabla T_e(X)/\nabla T_e(O)$ increases rapidly in the inner half island due to drastic changes between the X- and O-point profiles. In the outer half island, the ratio of $\nabla T_e(X)/\nabla T_e(O)$ is very low owing to small changes of the local T_e gradient from X- to O-point. Considering that the turbulence level is related to the local drive of the T_e gradient, the above results are in reasonable agreement with theoretical expectations.

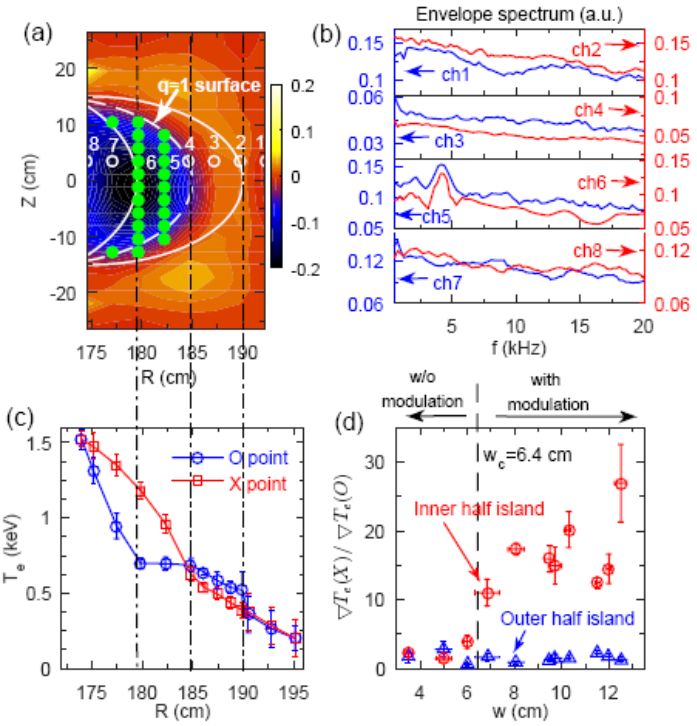

FIG. 5. (a) Effective modulation area on $\tilde{T}_e$ turbulence detected by the ECEI array (marked by green dots) at the inner half of the q=1 island; (b) envelope spectra of $\tilde{T}_e$ measured by eight ECEI channels at Z=3.46 cm, as indicated by white circles in (a); (c) radial profiles of T_e at the X-point (red) and the O-point (blue), measured by a multi-channel ECE radiometer in a wider radial range than the ECEI; (d) the ratio of $\nabla T_e(X)/\nabla T_e(O)$ as a function of the island width. The vertical line indicates a threshold width ($w_c \approx 6.4$ cm), above which the modulation of turbulence occurs.

The "uneven" T_e profile across the large TM island implies that the properties of the heat transport at the O-point are quite intricate. Here, we further survey the relation between the local T_e gradient and the turbulence level of $\tilde{T}_e$ detected by the ECEI across the O-point. The fluctuation data are taken at the phase-locked O-point starting from the onset of each O-point near the q = 1 surface for a duration of 100 μs (see Fig. 2(b)), and then averaged over 100 cycles for good statistics. Figures 6(a) and (b) show the temporal evolutions of the T_e fluctuation power, $\langle \tilde{T}_e^2 \rangle$, measured on several ECEI channels at Z = 3.46 cm across the O-point phase, and the radial profiles of $\langle \tilde{T}_e^2 \rangle$ are plotted in Figs 6(c) and (d). For the small island (w = 6 cm), the fluctuation power only shows a mild variation both inside and outside the TM island, as seen in Figs. 6(a) and

(c). In the case of large islands (w = 10.5 cm), Figs. 6(b) and (d) show significant changes of $\langle \tilde{T}_e^2 \rangle$ in different radial locations. At the inner location outside the island (R<179 cm), the fluctuation power is extremely high due to probably very steep T_e profile in that location (see O-point in Fig. 5(c)). Inside the island, the fluctuation power at the outer half region (185 cm<R<190 cm) is quite low, corresponding to small T_e gradient in that area. In this zone, the radial transport competes with the parallel one so that a finite temperature gradient persists inside the island [24].

However, at the inner half region (179 cm<R<185 cm), the level of $\langle \tilde{T}_e^2 \rangle$ is higher than that in the outer half, although the local T_e gradient is close to zero. Apparently, this high level of turbulence is not driven by the local gradient, but affected by "turbulence spreading" through mutual interaction of turbulent eddies [25-27], by which turbulence can propagate from a region where it is excited into a region where they may no longer be driven, or even suppressed. This mechanism allows turbulence to penetrate to the flattened O-point region from outside the island (R<179 cm), where the local gradient and fluctuation levels are both strong. With reduction of local gradient and free energy, the penetration terminates at q=1 surface, at which the magnetic connection length is short. In the spreading zone the turbulence level is relatively high (in comparison with outer half island), resulting in high-level outward thermal transport, and hence, the flattened T_e profile being maintained in the inner half region of the island.

It should also be noted that at the inner half island, the spreading turbulence at the O-point is significantly weaker than the turbulence driven by the large T_e gradient at the X-point. Therefore, the alternating change of the O- and X-point modulates the fluctuation amplitudes periodically, as shown in Fig. 2. In contrast, in the zone of the outer half island, the local T_e gradients between the X- and O-point are almost equivalent, which drive nearly the same level of turbulence, and thus, without giving modulation effects on local turbulence.

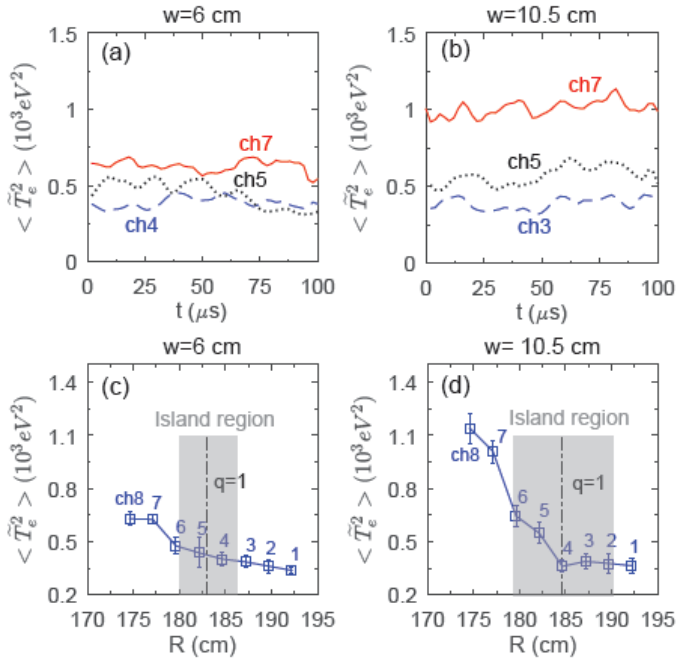

FIG. 6. Temporal evolutions of the T_e fluctuation power, $\langle \tilde{T}_e^2 \rangle$, measured on several ECEI channels at Z=3.46 cm across the O-point phase for two different island widths (a) w=6 cm and (b) w=10.5 cm. (c) and (d) show the radial profiles of $\langle \tilde{T}_e^2 \rangle$ measured by eight channels in Fig. 5(a) for w=6 cm and w=10.5 cm, respectively.

4. SUMMARY

In summary, we presented experimental results of modulation of electrostatic turbulence by rotating m/n=1/1 TM islands in the core of the HL-2A tokamak. Highly resolved 2D ECEI measurements show the first evidence that the turbulence modulation occurs solely for large islands and the modulation takes place only in the inner half area of the island due to significant alteration of local profiles and turbulence drives between the X- and O-point. Bi-spectrum analysis indicates strong nonlinear coupling between tearing mode and broadband turbulence. Experimental evidence also reveals that for large islands turbulence spreading takes place across the flatten O-point at the inner half island region. In the zone of the outer half island, the local T_e gradients and

turbulence drives between the X- and O-point are nearly equivalent, and hence, without modulating local turbulence.

ACKNOWLEDGEMENTS

The authors thank Prof. P. H. Diamond for useful discussion. This work is partly supported by National Key R&D Program of China under Grant No. 2017YFE0301106, 2014GB108000 and 2017YFE0301203, and by the National Natural Science Foundation of China under grant Nos. 11575057, 11705051, 11475057 and 11775070.

REFERENCES

[1] G. Fiksel et al., Phys. Rev. Lett. 75, 3866 (1995)
[2] S. Inagaki et al., Phys. Rev. Lett. 92, 055002 (2004)
[3] K. Ida et al., Phys. Rev. Lett. 88, 015002 (2002)
[4] K. J. Zhao et al., Nucl. Fusion 55, 073022 (2015)
[5] L. Bardóczi et al., Phys. Plasmas 23, 052507 (2016); ibid, 24, 056106 (2017)
[6] W. Suttrop et al., Nucl. Fusion 37, 119 (1997).
[7] E. Joffrin et al., Nucl. Fusion 43, 1167 (2003).
[8] T. Estrada et al., Nucl. Fusion 56, 026011 (2016).
[9] S. Günter et al., Nucl. Fusion 41, 1283 (2001)
[10] L. Bardóczi et al., Phys. Rev. Lett. 116, 215001 (2016)
[11] M.J. Choi et al, Nucl. Fusion 57, 126058 (2017)
[12] P.J. Sun et al, Nucl. Fusion 58, 016003 (2018)
[13] K. Ida et al Phys. Rev. Lett. 120, 245001 (2018)
[14] M. Jiang et al, Nucl. Fusion 58, 026002 (2018)
[15] L. Schmitz et al., Phys. Rev. Lett. 108, 155002 (2012)
[16] I. Shesterikov et al., Phys. Rev. Lett. 111, 055006 (2013)
[17] H. R. Wilson and J. W. Connor, Plasma Phys. Controlled Fusion 51, 115007 (2009)
[18] R. Fitzpatrick, Phys. Plasmas 2, 825 (1995); ibid, 23, 122502 (2016).
[19] A. B. Navarro, L. Bardoczi, T. A. Carter, F. Jenko and T. L. Rhodes, Plasma Phys. Control. Fusion 59, 034004 (2017).
[20] M. Jiang et al., Rev. Sci. Instrum. 84, 113501 (2013).
[21] Z. B. Shi et al., Rev. Sci. Instrum. 85, 023510 (2014).
[22] P. W. Shi et al., Plasma Science and Technology 18, 7 (2016).
[23] V. Igochine et al., Phys. Plasmas 21, 110702 (2014)
[24] W. A. Hornsby et al., Phys. Plasmas 17, 092301 (2010)
[25] X. Garbet et al., Nucl. Fusion 34, 963 (1994).
[26] T. S. Hahm et al., Plasma Phys. Control. Fusion 46, A323 (2004).
[27] R. E. Waltz and J. Candy, Phys. Plasmas 12, 072303 (2005).